Available online at www.sciencedirect.com
SCIENCE DIRECT®
ELSEVIER
Ultramicroscopy 103 (2005) 117–132
ultramicroscopy
www.elsevier.com/locate/ultramic

Dip Pen Nanolithography (DPN): process and instrument performance with NanoInk's NSCRIPTOR system

Jason Haaheim[a,*], Ray Eby[b], Mike Nelson[a], Joe Fragala[b], Bjoern Rosner[a], Hua Zhang[a], Greg Athas[a]

[a]*NanoInk, Inc., Corporate Office, 1335 W. Randolph Street, Chicago, IL 60607-1523, USA*
[b]*NanoInk, Inc., MEMS Fabrication, 215 East Hacienda Avenue, Campbell, CA 95008-6616, USA*

Received 20 May 2004; received in revised form 11 November 2004; accepted 22 November 2004

Abstract

Precision nanoscale deposition is a fundamental requirement for much of current nanoscience research and promises to facilitate exciting industrial applications. Tailoring chemical composition and surface structure on the sub-100 nm scale benefits researchers in topics ranging from catalysis, to biological recognition in nanoscale systems, to electronic connectivity on the nanoscale. Precision nanoscale deposition engenders applications such as additive photomask repair and nanodevice fabrication. Dip Pen Nanolithography™ (DPN™) is a scanning-probe-based direct-write technique for generating surface-patterned chemical functionality and discrete structures on the sub-100 nm scale. In this publication we explore the effects of changing tip radius and surface roughness. We find that blunter tips lead to higher minimum line widths and that higher rms surface roughness leads to higher minimum line widths; line edge roughness also increases with substrate roughness and surface feature size. Also, we characterize the performance of the NSCRIPTOR DPN instrument and demonstrate the placement of pattern features with precision better than 10 nm, and size control better than 15% for sub-100 nm features.

PACS: 07.79.Lh; 81.07−b; 81.16−c; 81.16.Nd

Keywords: Dip Pen Nanolithography (DPN); Scanning probe microscopy; Nanofabrication

1. Introduction

Much of what is today considered "nanotechnology" has been made accessible through the use of scanning probe microscopy (SPM) techniques, most notably atomic force microscopy (AFM) [1]. These methods descend from the invention of

*Corresponding author. NanoInk, Inc., Product Development, Corporate Office, 1335 W. Randolph Street, Chicago, IL 60607-1523, USA. Tel.: +1 312 525 2906; fax: +1 312 525 2972.
E-mail address: jhaaheim@nanoink.net (J. Haaheim).

0304-3991/$ - see front matter © 2004 Elsevier B.V. All rights reserved.
doi:10.1016/j.ultramic.2004.11.015

scanning tunneling microscopy in the early 1980s by Binnig and Rohrer [2]. While SPM includes direct observation of structures at molecular or atomic dimensions with the ability to measure many physical properties at this scale, scanning probe lithography (SPL) [3] involves actual fabrication of nanostructures using scanning probe techniques. SPL can be further categorized by additive, subtractive, and substitutive lithography.

Dip Pen Nanolithography™ (DPN™) [4] is an increasingly popular form of additive SPL and is now a commercialized process [5,6] involved in creating functional arrays and nanodevices [7,8]. The DPN process uses a coated scanning probe tip (the "pen") to directly deposit a material ("ink") with nanometer-scale precision onto a substrate (paper) [4,9]. It is an amazingly robust and versatile technique, and can deposit a variety of organic and inorganic molecules onto a variety of substrates [10] under ambient conditions (Fig. 1).

Table 1 provides an instructive look at DPNs place among nanopatterning techniques: it is highly scalable with the use of multi-pen arrays; it is a technique that enables both bottom up nanofabrication (self-assembly, templating) [11] and top down resist-based techniques [12]; and it is high resolution (14 nm). DPN is a direct-write technique, so materials of interest can be placed exactly (and only) where desired, without the use of a mask. Among sub-50 nm techniques—such as e-beam lithography—DPN is the only one that can directly deposit molecules under ambient conditions [4,9,13-14]. In addition, because NanoInk's nanolithography platform—the NSCRIPTOR™—is based on SPM technology, it is inherently capable of both pattern fabrication and immediate verification of the result by imaging.

Previous DPN efforts have demonstrated 15 nm features [14], and herein NanoInk demonstrates mercaptohexadecanoic acid (MHA) lines on gold with 14 nm line widths. When using oligomer or protein-based inks, the DPN method can produce nanoscale spotted features which are much smaller than conventional bio-arrays [15,16]. For example, Mirkin and co-workers [17] generated Lysozyme and Immunoglobulin G (IgG) nanoarrays. The

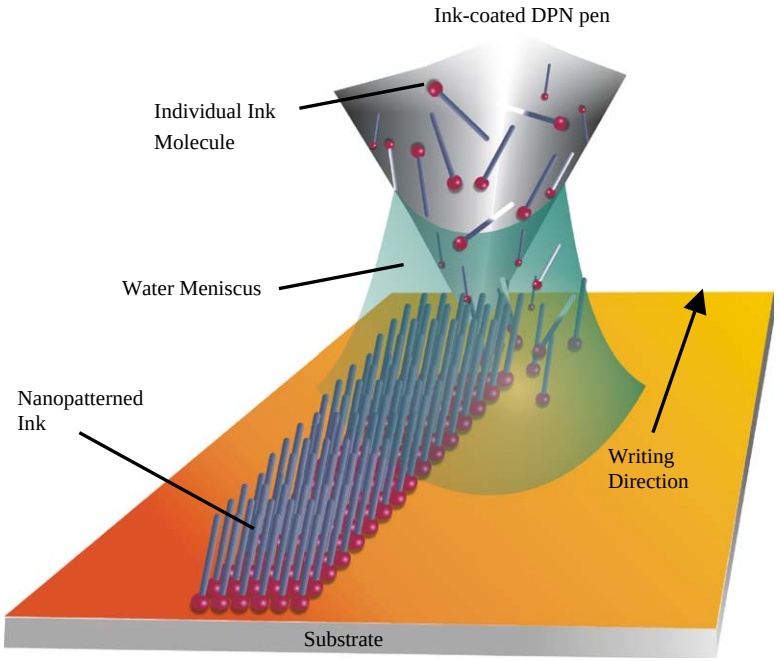

Fig. 1. Schematic of the DPN process. A molecule-coated AFM tip deposits ink via a water meniscus onto a substrate.

Table 1

	Nanopatterning technique	Serial/ parallel	Material flexibility	Resolution	Accuracy	Speed	Cost	
							Equipment	Operating
Top down	Photolithography	Parallel	No	~90 nm	High	Very fast	$10M++	High
	E-beam lithography	Serial	No	~15 nm	High	Medium	$1M–$20M	High
	Nanoimprint lithography (NIL)	Parallel	No	~10 nm	High	Fast	$1.6M	High (fabrication of masters)
Enables both	Dip Pen nanolithography (DPN)	Serial or parallel pens	Yes	14 nm	Extremely high	Slow, but highly scalable	$200k	Low
Enables both	Microcontact printing (μCP)	Parallel	Yes	~100 nm	Low	Fast	$200k	High (mask sets)
Bottom up	Scanning tunneling microscopy (STM)	Serial	Limited	Atomic/ molecular	Extremely high	Very slow	~$200k–$1M	Low

arrays featured structures as small as 100 nm in diameter and were shown to exhibit an almost complete absence of non-specific binding of proteins to the passivated areas of the structure. Additional applications of DPN include, but are not limited to, using DPN patterns as etch resist [12,18–20], and the creation of templates for subsequent particle attachment [21,22].

In a recent review paper [23], Ginger et al. categorized DPN applications according to four broad areas: (1) biomolecular micro- and nanoarrays; (2) controlling biorecognition processes from the molecular to cellular level; (3) DPN templates for orthogonal assembly of nanostructured materials; and (4) DPN-patterned etch resists. The authors would also like to propose additive repair technology, and direct deposition and manipulation for nanoelectronic characterization. This study is pertinent to all of these areas in that many of the data and conclusions contained herein are both platform—and chemistry-general—we discuss factors affecting basic diffusion, factors not tied to any specific chemistry.

The goals of this current study are twofold. First, we wish to provide a complement to previous DPN work [10,24–26] where the effects of varying environmental conditions were studied while keeping the tip and substrate the same. Here, we maintain stable environmental conditions (temperature and relative humidity) but explore the DPN process effects of varying tip radius and substrate roughness. Second, we introduce cutting edge technology to the research community that allows access to this versatile bottom-up nanofabrication technique on a repeatable basis; as such, we demonstrate that NanoInk's DPN system, the NSCRIPTOR, is capable of performing to the exacting demands of nanoscience research. Particularly, we explore the process performance (factors affecting feature deposition and measurement) and instrument performance (hardware and software capabilities).

2. DPN process performance: experiments and results

All experiments were performed using the NSCRIPTOR system, which includes an environmental chamber capable of controlling temperature (from $-2\,^{\circ}C$ below room temperature to $10\,^{\circ}C$ above room temperature) and relative humidity (RH) (0–75% RH) through a real-time feedback loop. Environmental conditions were kept constant ($\pm 0.1\,^{\circ}C$, and $\pm 0.5\%$ RH) throughout all experiments. The NanoInk E-Chamber software permits environmental stabilization while being able to avoid associated noise by turning off the

heater, fan, and nebulizer during writing and imaging. Oxide sharpened DPN pens were provided by the NanoInk MEMS facility (Campbell, CA). All of the tips were then coated with the alkanethiol MHA by dipping into a 5 mM solution of MHA in acetonitrile. We used three different Au substrates: mica-peeled (and therefore clean until the time of writing), evaporated, and sputtered. The evaporated and sputtered samples were stored under argon in methanol-cleaned eppendorf tubes.

DPN experimentation was automated by NanoInk's InkCAD^{TM} software. InkCAD controls when the MHA-coated tip is in contact with the surface, and how long it dwells (creating dots) or how fast it moves (creating lines). Further, the ink diffusion process was calibrated according to a routine called InkCal^{TM}. Many studies [4,24–27] have demonstrated that alkanethiol feature sizes depend on dwell time or tip speed. InkCal automates the process of drawing dots and lines at a range of dwell times and tip speeds, then guides the imaging of features, the measurement of feature sizes, and finally plots the data to obtain a diffusion coefficient (C) expressed in $\mu m^2/s$. In addition, it has been previously noted [24] that the diffusion behaves differently during the deposition of dots as opposed to lines. With dots, there is a static diffusion scenario in which ink diffuses from a source, and then continues to diffuse as the self-assembled monolayer (SAM) forms outward from the tip. With lines, however, we have a dynamic scenario in which ink at the leading edge of motion is always seeing fresh attachment sites on the gold, and ink on the trailing edge is still diffusing over itself. As such, the InkCAD software accounts for this by allowing independent calibration of dots and lines, each having its own ink model and diffusion constant.

As mentioned, previous DPN work [10,24–26] varied environmental conditions while keeping the tip and substrate the same. While exploring minimum line width dependencies on surface roughness and tip radius, we kept environmental conditions stable at $T = 24.9 \pm 0.1\,^{\circ}C$ and $RH = 39.7 \pm 0.5\%$. Resulting diffusion constants ranged from $C = 0.029$ to $0.085\,\mu m^2/s$. Unless otherwise noted, all DPN data are lateral force microscopy (LFM) scans obtained with the NSCRIPTOR.

2.1. Minimum line width vs. substrate roughness

For this study we used only sharpened tips. (NanoInk oxide sharpened silicon nitride D-type multi-probe array, A3B probes. Tip radius 12–15 nm.) The force between the tip and substrate was kept the same from experiment to experiment by using the same setpoint and laser alignment conditions. Patterning times were less than 90 s according to the tip speeds discussed below, and the ink diffusion constant. We also maintained constant temperature and relative humidity. Fig. 2 compares the three different gold surfaces used in this experiment. It should be noted that the mica-peeled gold has spurious surface defects (i.e., Figs. 3a, 8a and b) which frequently form during the peeling process. Importantly, it is possible to find large regions in between this debris that are atomically flat. These represent the true nature of the surface—the debris is statistically insignificant and does not noticeably affect diffusion. This is in contrast to evaporated gold which is generally more uniform, but measures a higher overall roughness (leaving sputtered gold as the roughest option). Additionally, our data suggests that the lateral size of gold features increases with surface roughness. Figs. 2b and c show that individual sputtered gold features have a larger area than the evaporated features.

As seen in Fig. 3, we measure higher minimum line widths for rougher gold. Fig. 4a shows this dependence more explicitly. For all three gold substrates in Fig. 3, after certain tip speeds (1.5–3.0 μm/s) the lines do not get any thinner, only fainter (meaning that a smaller amount of MHA molecules were deposited on the Au). As will be elaborated below, this seems to indicate we are truly measuring the minimum line width—a lithography parameter dictated by the minimum tip–meniscus–substrate interaction area. Line width measurements were made using the line-cursor measurement tool in InkCAD, seen in Fig. 5. This tool is quite accurate and consistent in terms of providing line width measurements, especially if the edge of a line is not clearly

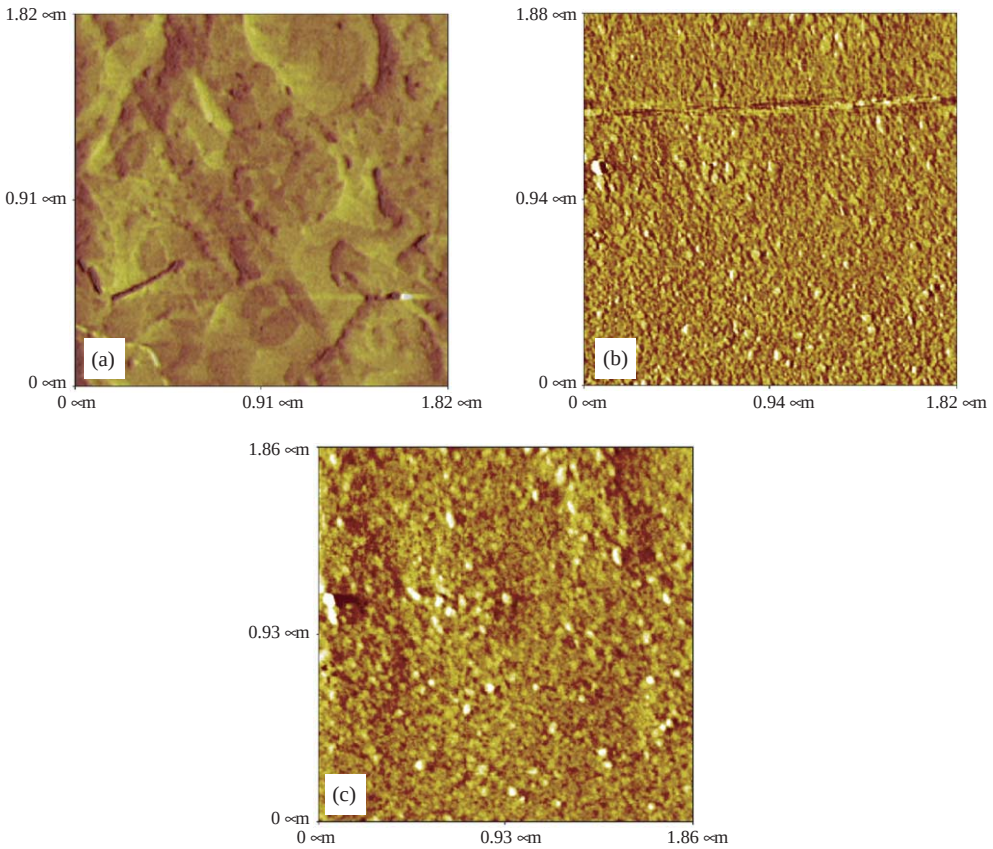

Fig. 2. Error signal images of gold substrates: (a) mica-peeled gold illustrating atomic terraces, rms roughness $\leqslant 3$ Å; (b) evaporated gold, rms roughness = 0.7 nm; (c) sputtered gold, rms roughness = 1.1 nm (rms roughness data were obtained from topographic counterparts to these error signal images).

defined. The tool allows one to average these effects, and has proven much more consistent and meaningful than a simple LFM line scan.

We initially considered that rougher surfaces may restrict the diffusion of ink, thus resulting in narrower minimum line widths. As shown in Fig. 4b, the surface feature boundaries do indeed restrict ink flow (resulting in lower C values), but this results in higher minimum line widths (Figs. 3 and 4a). While this effect presents avenues for further study, we propose several possible explanations. It is known that a water meniscus' contact angle decreases with increasing surface roughness [28]. This means that the meniscus contact area increases with surface roughness. Given that the meniscus facilitates ink diffusion, this could explain the higher minimum line widths we observed for rougher surfaces. Furthermore, a rougher substrate not only forces the ink to diffuse along a more tortuous path, it can also laterally perturb the tip's forward motion (see Fig. 6a). An analogous situation would be to compare writing with a fine-point pen on printer paper versus 80 grit sandpaper; as the pen is drawn across the sandpaper surface, the tip is laterally "jostled" by the surface features resulting in an apparently wider, smeared line. Similar effects have been observed on molybdenum disulfide (MoS_2) surfaces according to stick–slip behavior across atomic lattice sites [29]. Another possible explanation has to do with surface contact points.

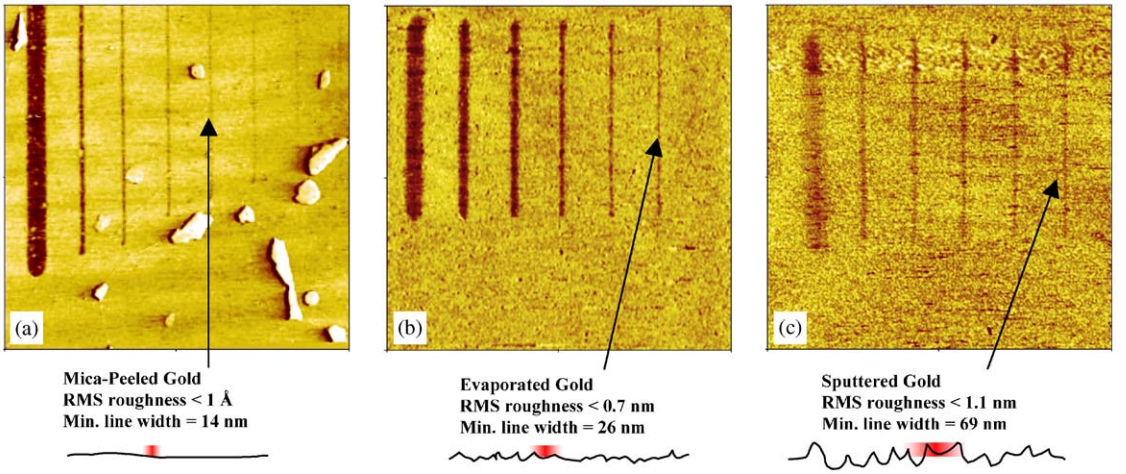

Fig. 3. Reverse LFM images (R→L) of MHA lines written with a sharpened tip on: (a) mica-peeled gold, yielding 14 nm minimum line width, $C = 0.043$, 4.0 μm scan; (b) evaporated gold, yielding 26 nm minimum line width, $C = 0.040$, 7.0 μm scan; and (c) sputtered gold, yielding 69 nm minimum line width, $C = 0.029$, 6.6 μm scan. Note that the diffusion constants decrease with increasing surface roughness.

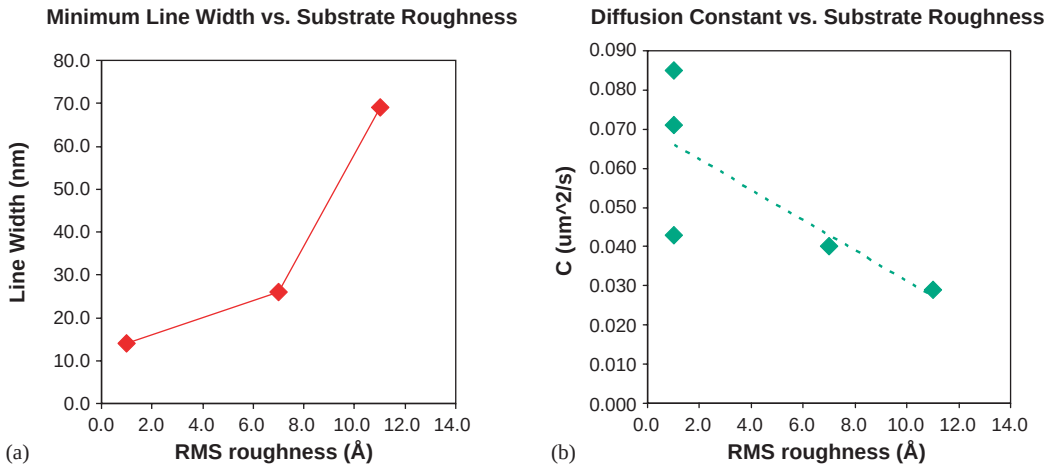

Fig. 4. (a) Plot of minimum line width vs. substrate roughness, showing higher minimum line widths for rougher surfaces. (b) Plot of diffusion constant vs. substrate roughness, showing the generally higher diffusion constants for smoother surfaces. A rough linear fit is shown to emphasize the trend.

It has been shown [30] that a tip on a perfectly smooth surface can form a single asperity contact; however, as the surface roughens there are multiple asperities contact. Fig. 6b shows a possible distribution of asperities according to surface feature size. Larger features would form asperities contact that are further apart. Since our data indicates that surface feature size increases with surface roughness, rougher surfaces can correspond to a larger effective contact area, and thus wider lines. It is further possible that the ink diffuses according to these surface feature sizes. An analogous situation would be pouring water in ice cube trays. Since the water has distinct locations it can occupy, water in a tray with larger ice cubes will cover a larger area. Fig. 6c illustrates

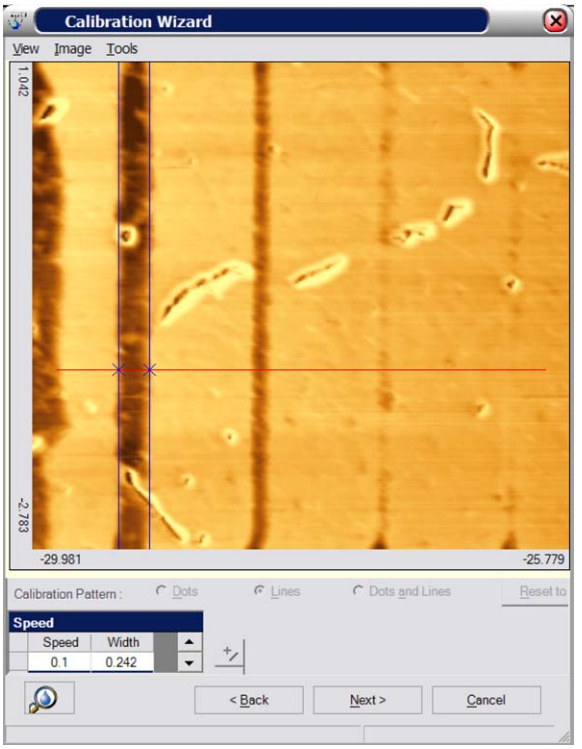

Fig. 5. Demonstration of feature size measurement technique using the line-cursor measurement tool in InkCAD. The tool is accurate and consistent in terms of providing line width measurements. Because the tool allows the eye to average across the entire cursor-line, we obtain more consistent and meaningful measurements than by using arrows placed across a single line scan profile.

how this could possibly apply to MHA diffusion on Au.

2.2. Minimum line width vs. tip end radius

For this study we used mica-peeled gold substrates, along with constant temperature and relative humidity. Patterning times were less than 90 s according to the tip speeds discussed below, and the ink diffusion constant. Fig. 7 illustrates the concept we propose and validate—tips with larger radii will lead to larger minimum line widths. For a blunter tip, the minimum tip–meniscus–substrate interaction area is larger, and thus it follows that minimum line widths will be higher. This behavior is seen in Fig. 8, where we used four different tips to demonstrate this effect (tip radius and line width data is summarized in Fig. 9): (1) an oxide sharpened tip; (2) an unsharpened tip (no oxide sharpening); (3) a super-unsharpened tip (one that has been intentionally etched to produce a truncated pyramidal tip); and (4) an unsharpened tip coated with PDMS (a DPN stamp tip) according to the method described elsewhere [31]. In fact, the DPN stamp tip was noticeably duller than the other three; its tip radius was large enough that small surface features appeared very large as a result of the tip–sample convolution.

Similar to the phenomenon noted above, after exceeding a certain tip speed (for all four tips) the lines do not get any thinner, only fainter. This provides further evidence that we are truly measuring the minimum line width—a lithography parameter dictated by the minimum tip–meniscus–substrate interaction area. When the tip moves faster, the deposition/diffusion enters an ''intermittent writing'' regime wherein the ink is no longer continuously diffusing from the tip and uniformly self-assembling on the surface. The tip speed across the surface is faster than the maximum rate of uniform attachment, and thus we observe patchy deposition. This is particularly evident in Fig. 8b and c, where the threshold is between 1.5 and 3.0 μm/s. The limit of this regime is zero apparent deposition, with evidence of only writing at the end points (seen in Fig. 8c and d) where the tip takes a finite amount of time to approach and retract. This regime becomes useful when imaging with an inked tip.

2.3. Summary of DPN's substrate and tip dependencies

As shown, rougher substrates lead to higher minimum line widths (Fig. 4a). The narrowest line widths (14 nm) have been achieved on mica-peeled gold. Additionally, the rougher substrates tend to inhibit diffusion as can be seen in the decreasing diffusion constants (Fig. 4b), and the uniformly high diffusion constants of mica-peeled gold. Similarly, blunter tips will yield higher minimum line widths (Fig. 9). The narrowest line widths have been achieved using NanoInk's oxide sharpened tips (radius 12–15 nm).

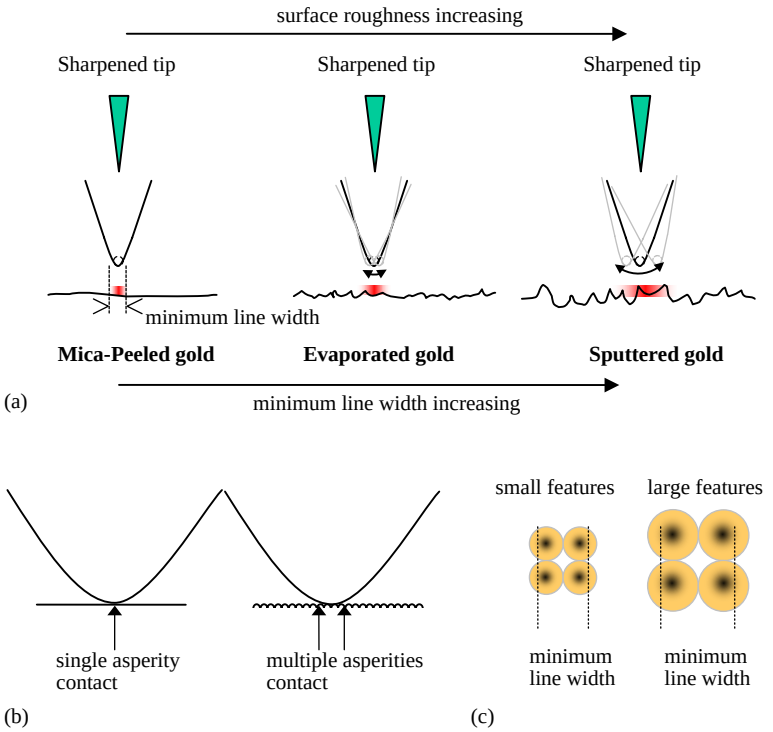

Fig. 6. Possible explanations for the observed minimum line width dependence on surface roughness: (a) as the pen is drawn across the substrate, the tip is increasingly "jostled" laterally by the rougher surface structure, resulting in higher minimum line widths; (b) a tip on a perfectly smooth surface can form a single asperity contact. As the surface roughens, multiple asperities contact form, corresponding to a larger effective contact area; and (c) our data indicates that surface feature size increases with surface roughness. It is possible that the ink diffuses according to these sizes.

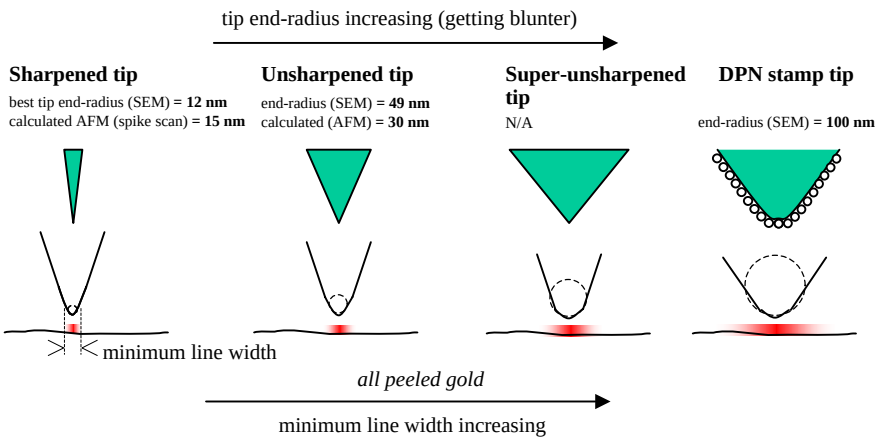

Fig. 7. Illustration of minimum line width dependence on tip sharpness. Larger tip radii have a higher minimum tip–meniscus–substrate interaction area, leading to higher DPN minimum line widths for blunter tips.

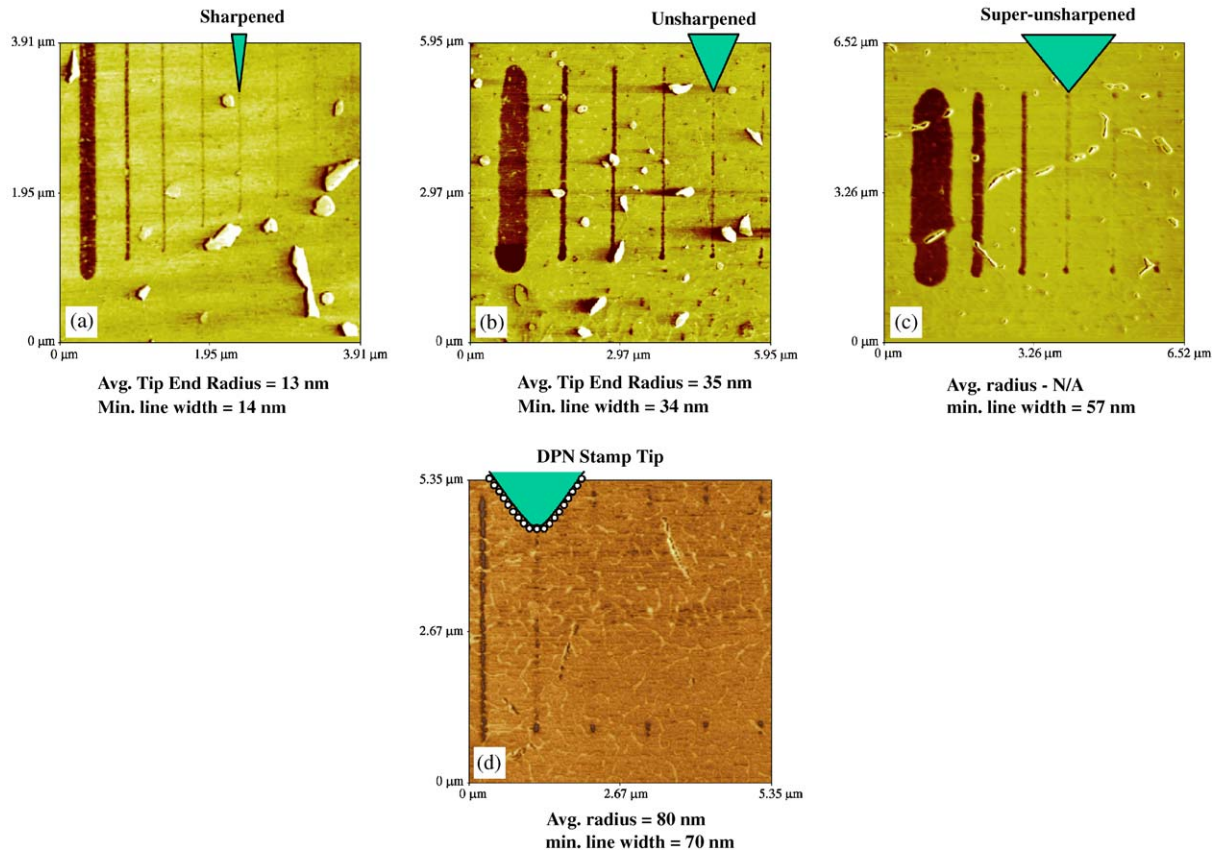

Fig. 8. Reverse LFM (R→L) images of MHA lines written on peeled gold with: (a) sharpened tip, yielding 14 nm minimum line width, $C = 0.043$; (b) unsharpened tip, yielding 34 nm minimum line width, $C = 0.071$; (c) super-unsharpened tip, yielding 57 nm minimum line width, $C = 0.085$; and (d) DPN stamp tip (PDMS coated), yielding 70 nm minimum line width, $C = 0.395$. (This diffusion constant is extremely high, most likely due to the different diffusion mechanism arising from the way that ink can be stored within the PDMS on the tip.) Note that the diffusion constants here on peeled gold are consistently higher than evaporated gold ($C = 0.040$) and sputtered gold ($C = 0.029$), given the same environmental conditions.

In general, the minimum line width is not equal to but proportional to tip radius. This is because of the effective contact area determined by tip–meniscus–substrate interaction, and that the meniscus likely provides diffusion outside the immediate contact area of the tip. Additionally, tip contact area is not the same as tip radius (though they are certainly related). In terms of DPN, the tip–meniscus–substrate interaction area likely involves the tip contact area, the meniscus, and can be affected by factors such as tip speed and humidity. There have been several studies exploring alkanethiol diffusion [24–27] and, notable for our case, it has been shown that the water meniscus does not fully form at high tip speeds [32]. This suggests a regime of tip speeds in which the meniscus is present, but the interaction area with the substrate is smaller. Due to the nature of the tip–meniscus–substrate interaction area for high writing speeds (narrow lines), the narrowest continuous lines give us an accurate (if slightly inflated) measurement of our tip end radius.

Thus, mica-peeled gold and sharpened tips give the greatest lithography control—the narrowest lines and generally best contrast (since the substrate is perfectly clean until the moment it is peeled). Figs. 3a and 8a both show the finest narrow lines written (14 nm) using an oxide

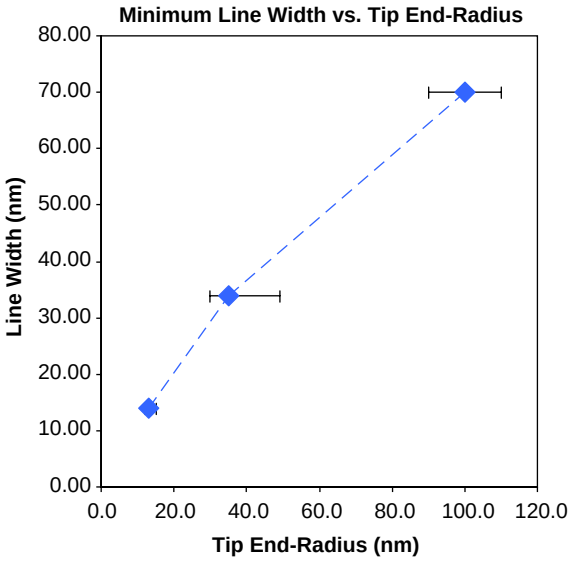

Fig. 9. Plot of minimum line width vs. tip radius, showing higher minimum line widths for blunter tips. Error bars are based on SEM and/or AFM measurements.

sharpened tip on mica-peeled gold. The literature reports 15 nm diameter dots [14] , but it should be noted that the work was done using MHA on Au (1 1 1) that was passivated by ODT (octadecanethiol). Mica-peeled gold also generally gives the highest diffusion constants, since there is far less impeding the ink's lateral movement across the surface. Moreover, our data shows that for a given set of environmental conditions, the diffusion constant will decrease with increasing surface roughness.

2.4. Line edge roughness

In micro- and nanofabrication, an increasingly important lithography quality parameter is line edge roughness (LER). Here we will briefly address this parameter as it pertains to DPN. Under the lithography conditions detailed above, we printed the MHA line patterns shown in Fig. 10

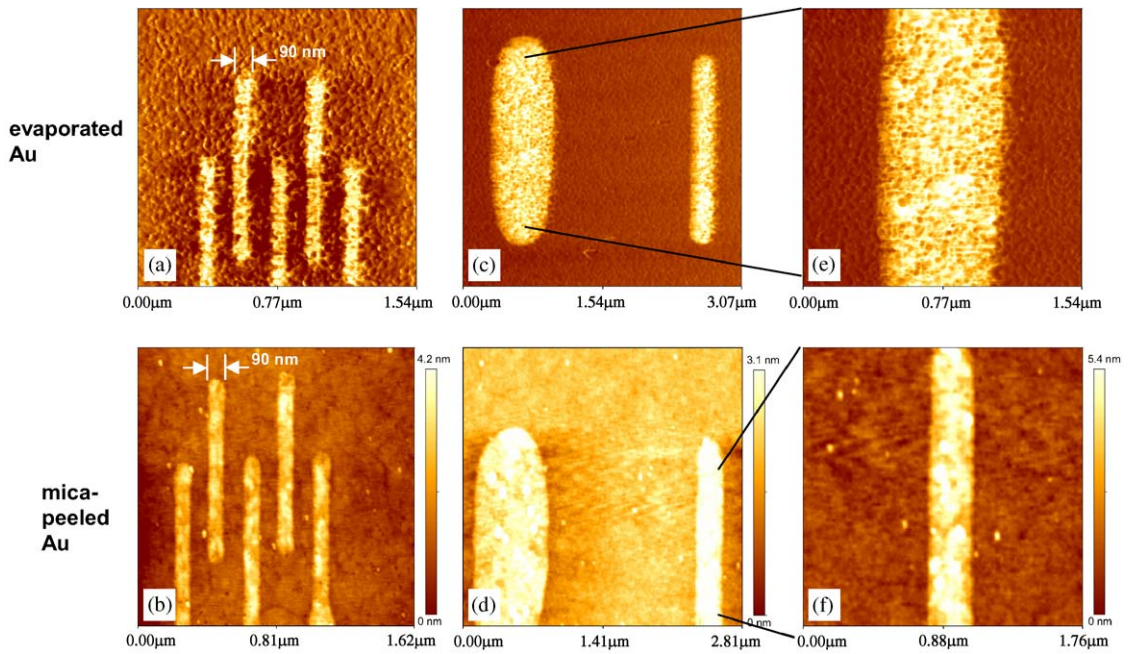

Fig. 10. MHA lines written on gold with a sharpened tip. (a,c,e) Forward LFM (L→R) images showing distinct LER, and (b,d,f) the same lines on mica-peeled gold showing much smoother line edges (AC mode topography images). AC mode imaging was performed on the NSCRIPTOR using probes by NanoWorld.

on both evaporated and mica-peeled gold. We initially characterized the patterns using AC mode (non-contact) to define topography. We then passivated the samples with ODT to prevent any latent MHA diffusion, and imaged the patterns in contact mode (LFM). Tip exchange and realignment were facilitated by InkCAD's nanoscale alignment routines. A comparison between the evaporated and mica-peeled gold patterns is striking, but not unexpected given our arguments above discussing ink diffusion on various substrates. Fig. 10e clearly shows how the ink diffuses along a tortuous path dictated by the surface feature boundaries. This in turn leads to line edges where LER is determined by lateral surface feature size. Contrast this to Fig. 10f and note that mica-peeled gold, absent of distinct surface features, allows far smoother line edges to be patterned.

Our measurement technique quantifies this difference. To measure LER, we define the "roughness envelope" as the width of the cursors shown in Fig. 11. As discussed in Fig. 5, this allows accurate and consistent measurements since the eye is able to effectively average across the entire cursor line, as opposed to arrows placed across a single scan line profile. MHA lines on this evaporated gold sample measure LER = 39 nm, whereas the mica-peeled gold sample lines measure LER = 14 nm.

We conclude that LER correlates to lateral surface feature size, and that larger features yield rougher line edges. We should note, however, that LER characteristics are somewhat DPN-process dependent and do not necessarily speak to the NSCRIPTOR's patterning capability. Generally, for high diffusion conditions (high temperature, high humidity, and/or low rms roughness) the integrity of patterned dots and lines will decrease and LER will increase (note particularly Fig. 8c, showing a rough line on peeled gold under high diffusion conditions), but these process behaviors merit further study. However, regularity of line widths and dot sizes can be improved by electrochemical "whittling" [33] .

2.5. Small area, small feature imaging

As has been noted above, high tip speeds usually result in either very thin or intermittent lines. For the highest tip speeds it has been shown that the meniscus does not fully form [32]. For this reason, it is possible to both write and image with the same inked tip. (For example, a 10 μm scan at 4 Hz moves the tip at 80 μm/s, an order of magnitude higher than the intermittent writing threshold of 1.5–3.0 μm/s seen in Fig. 8b and c.) As such, all LFM images were generated in this fashion.

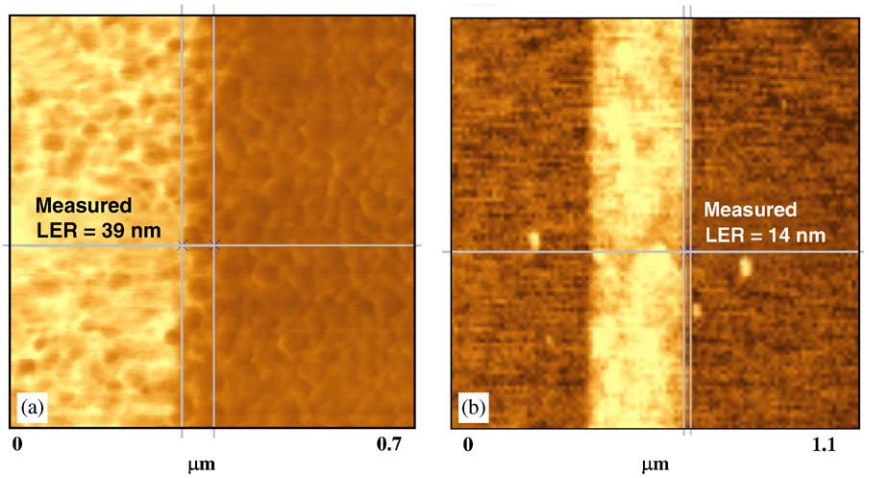

Fig. 11. LER measurement technique on (a) zoom of Fig. 10e (evaporated gold), with 39 nm LER, and (b) zoom of Fig. 10f on mica-peeled gold with 14 nm LER. As discussed above, line cursors yield more consistent meaningful measurements of LER than arrows placed across a single line scan profile.

Intermittent writing becomes problematic, however, for the small scan sizes ($<2\,\mu m$) used to resolve very small features. Even with high scan speeds, enough intermittent deposition will be spatially close enough to cover the scanned area. In fact, when scanning a $1 \times 1\,\mu m^2$ square at 4 Hz with 512×512 resolution, the tip's net scan time is 2 min. (In this case, the scan rate of the tip is $8\,\mu m/s$ which is much closer to the intermittent writing threshold of 1.5–3.0 μm/s.) This means the tip spends 2 min on the surface within a $1 \times 1\,\mu m^2$ square. Moreover, at the edge of the scan range the tip experiences a definite deceleration, followed by an acceleration in the opposite direction. This means the tip speed is less than 8 μm/s at the edges of the scan range. These effects result in MHA filling in the entire area and obscuring feature contrasts. This is particularly evident when doing a large scan, and then zooming in for a smaller scan of detailed features: the frictional contrast in the smaller scan is greatly diminished because the tip has already coated the entire surface. Inevitably, this affects how well one can actually measure the smallest DPN pattern features. There are several solutions to this problem: (1) image with a clean tip; (2) image with another molecule-coated tip with different surface hydrophilicity. For example, if patterning with MHA (hydrophilic), image with an ODT (hydrophobic) coated tip; (3) image in AC mode; or, (4) for the ultimate solution with greatest convenience (avoiding tip changing), one can use multi-probe arrays. In this case, one can dip only the "writer" probe into inks (using Inkwell arrays) while leaving the "reader" probe clean (i.e., undipped). With this accomplished, only minor x–y translation is required between making patterns with the writer probe and inspecting them with the reader probe.

3. Nscriptor instrument performance: experiments and results

Here we demonstrate that a commercial DPN system is capable of performing to the exacting demands of nanoscience research. Several measures are critical as necessary proofs of a robust nanolithography system: minimum pitch placement, placement precision, feature size precision, and feature size accuracy. We were able to demonstrate DPN patterning to exacting standards, therefore validating that the instrument used is capable of high-performance nanoscale lithography. We applied the experimental methods based on the conclusions of Section 2; i.e., we used oxide sharpened tips on mica-peeled gold. Environmental conditions were kept stable at $T = 24.9 \pm 0.1\,^{\circ}C$ and $RH = 39.7 \pm 0.5\%$ throughout all experiments.

3.1. Minimum pitch

We tested how closely the system could place features and still resolve them, and how reliably it could do so. We determined that patterns of interdigitated lines, systematically narrower and closer together, would yield optimal results. Fig. 12 shows the results of this test. Essentially, the instrument can place features with a pitch smaller than can be measured. The limiting factor is the narrowest lines of 14–20 nm. Thus, we can confidently say the instrument can accurately place features within 20 nm of each other. In reality, it is likely that the instrument can reliably place objects much closer; this will be proven with future capability for patterning even smaller feature sizes.

3.2. In-layer placement precision

In addition to a minimum pitch of 20 nm, we see that the instrument is very uniform in its placement of these features (Fig. 12). The standard deviations of the pitches are less than 5 nm in all cases. From this, we can easily say that the instrument can perform with an "in-layer" placement precision better than 10 nm. ("In-layer" refers to features patterned during a single lithography job with the same inked pen.)

3.3. Feature size precision

Fig. 13 illustrates an excellent case of precise feature size lithography. This is a measure of the instrument's ability to consistently repeat a feature size. There are 45 lines printed, all with line width standard deviations below 10%. Also note

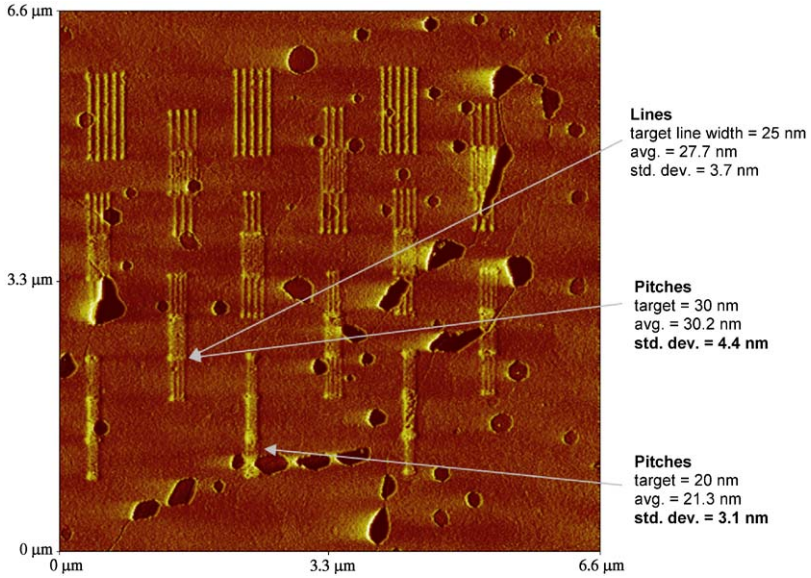

Fig. 12. Forward LFM (L→R) image of interdigitated DPN line patterns of MHA written onto mica-peeled gold using a sharpened tip; $C = 0.060$. Total patterning time = 44 s. We observe pitches down to 20 nm, and placement precision better than 10 nm according to standard deviation measurements.

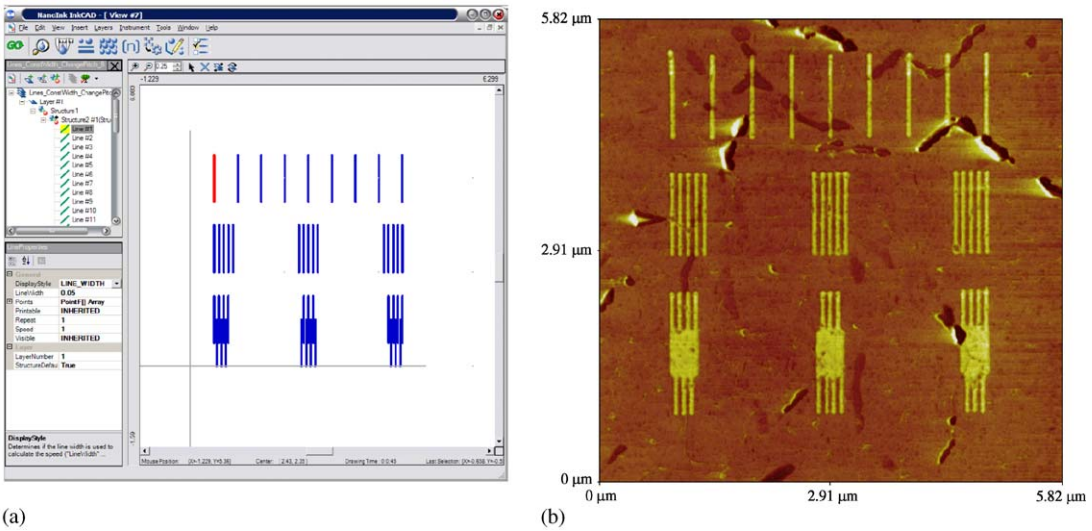

Fig. 13. (a) InkCAD-generated interdigitated line patterns, set to 50 nm line widths. (b) Forward LFM (L→R) image of 45 MHA line patterns written on mica-peeled gold using a sharpened tip; $C = 0.029$. Total patterning time = 78 s. Note the precise pitch placement down to 50 nm, and extremely precise feature sizes (line width measurements standard deviation $<10\%$).

that these line widths are set to 50 nm. In general, feature size precision for both dots and lines is better than 15% for sub-100 nm features, and better than 5% for features above 100 nm. However, the issue of how close we get to our target line width is one of feature size *accuracy*.

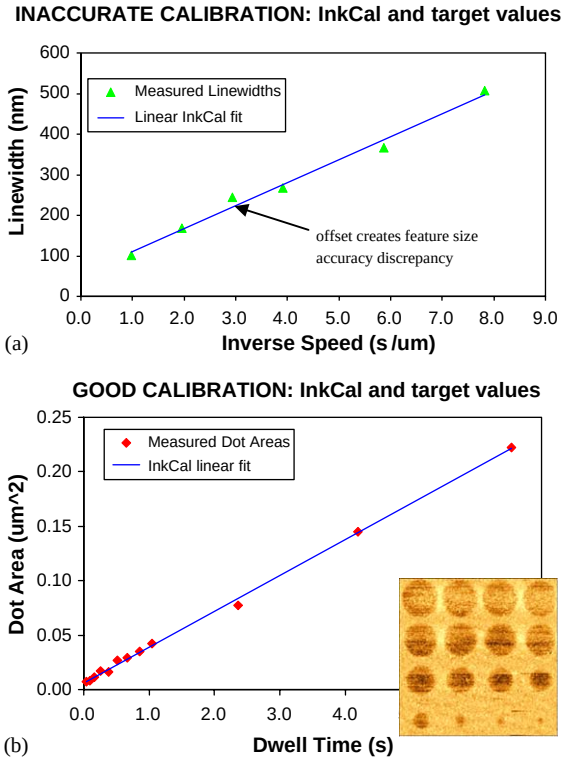

Fig. 14. (a) Plot of line width vs. inverse tip speed illustrating the experimental conditions for an inaccurate ink calibration. (b) Plot of dot area vs. dwell time illustrating a good calibration ($C = 0.033$), which will lead to accurate writing of feature sizes; inset: array of dots used for calibration.

3.4. Feature size accuracy

The accuracy of patterned features was also determined; this is a comparison between designated feature sizes, and their actual measured size. This result depends on the quality of ink calibration and the degree of process stability. As noted in Section 2, we perform an ink diffusion calibration (InkCal) doing DPN experiments. InkCal involves drawing dots and lines at a range of dwell times and tip speeds in order to obtain the final diffusion coefficient. While previous studies [4,24–27] have demonstrated varying diffusion behavior with a variety of theoretical models, the nature of the data in InkCal is generally linear (seen in Fig. 14). The quality of the data used for calibration determines the accuracy with which one can pattern features of a specified size; data that deviates from a fit will lead to an inaccurate calibration (Fig. 14a). There are several factors to consider in order to perform a good calibration. One must calibrate diffusion under a stable environment; temperature and humidity fluctuations will alter the behavior of ink diffusion and invalidate the calibration. High-quality, high-contrast patterns are more conducive to accurate feature size measurement; conversely, poorly resolved or irregular DPN features will generally lead to inaccurate size measurements. Finally, one should acquire at least 5 data points—enough so that a diffusion trend (whether linear, or non-linear) will be evident and the software can make a fit to this data. Following these requirements (see Fig. 14b data), we can achieve accuracy to within 1% of a specified feature size (Fig. 15). This data shows a pattern with a 100 nm designated line width, and when measured yields an average line width of 101 nm.

4. Summary and outlook

In conclusion, this paper has addressed DPN process and instrument performance with NanoInk's NSCRIPTOR DPN system. Pitch, precision, and accuracy tests are platform-specific and demonstrate the limits of nanoscale lithography while done on a specific system. The systematic DPN studies regarding tip radius and substrate roughness are both platform—and chemistry—general in that they demonstrate fundamental characteristics and limits of ink diffusion behavior. This work is a complement to previous DPN work that kept tip and substrate conditions the same while varying environmental conditions. We have shown that both blunter tips and rougher gold substrates yield higher minimum line widths. We have demonstrated that DPN with characterized oxide sharpened silicon nitride probes on mica-peeled gold substrates will yield optimal lithography conditions, producing the smallest feature sizes and best resolvable contrast from imaging. We have demonstrated 14 nm line widths under these conditions. The mica-peeled gold provides the highest diffusion constants, and our data

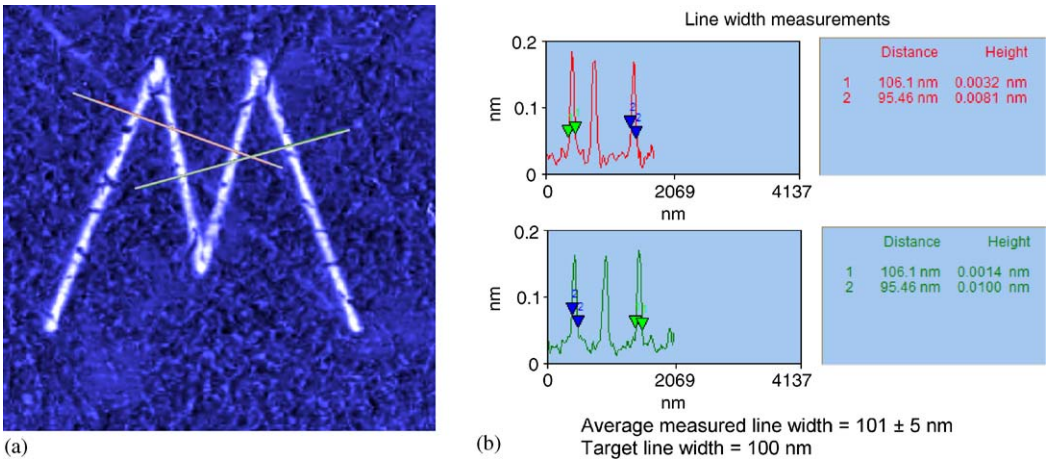

Fig. 15. (a) Forward LFM (L→R) image of MHA line patterns written on evaporated gold using a sharpened tip, 4 μm scan. The InkCAD generated pattern was targeted for 100 nm line widths. Line traces indicate measurement cross-section lines. (b) Measurement cross section data demonstrating an average measured line width of 101 ± 5 nm. The average is within 1% of the target line width, with an error of ±5%. *Note*: in this case an ink calibration was performed prior to the experiment which met all the conditions of a "good" calibration.

indicates that diffusion constants decrease with increasing surface roughness.

We also introduce the NSCRIPTOR™ as a nanolithography platform system that performs the DPN process on a repeatable and controllable basis. We characterized this instrument showing nanometer feature placement precision, and nanoscale feature size precision and accuracy. The system can achieve line grid pitches down to 20 nm, with placement precision better than 10 nm. Feature size precision is 15% for sub-100 nm features, and 5% for features above 100 nm. With a carefully performed ink diffusion calibration, feature size accuracy can be better than 1%.

The emerging field of nanotechnology requires a set of specific bottom-up capabilities; the DPN process fills this fundamental need for controlling the placement of molecules at the nanoscale, and forms a critical path towards the manipulation of nanomaterials and the future developments and applications of nano/bio devices. DPN is an active field of research and NanoInk is dedicated to further its cause. New chemistries are being developed that provide inks with desired electrical, optical, and biological properties. Probe arrays with individually actuated probes are now offered that further increase patterning versatility. We believe that DPN is a core technology for exciting new research and prototyping in the growing field of nanotechnology.

Acknowledgments

This work would not have been possible without the previous and continuing DPN research and MEMS development efforts of the Mirkin research group at Northwestern University and the group of Chang Liu at the University of Illinois at Urbana-Champaign. The authors would also thank all the employees at NanoInk.

References

[1] G. Binnig, C.F. Quate, C. Gerber, Phys. Rev. Lett. 56 (1986) 930.
[2] G. Binnig, H. Rohrer, C. Gerber, E. Weibel, Appl. Phys. Lett. 40 (1982) 178.
[3] S. Kramer, R.R. Fuierer, C.B. Gorman, Chem. Rev. 103 (11) (2003) 4367.
[4] R.D. Piner, J. Zhu, F. Xu, S. Hong, C.A. Mirkin, Science 283 (1999) 661.
[5] Nanoink, 1335 W. Randolph St., Chicago, IL 60607, www.nanoink.net.

[6] C.A. Mirkin, R.D. Piner, S. Hong, Methods utilizing scanning probe microscope tips and products therefore or products thereby, US Patent, #6635311, 2003.
[7] L. Fu, X.G. Liu, Y. Zhang, V.P. Dravid, C.A. Mirkin, Nano Lett. 3 (6) (2003) 757.
[8] M. Su, S.-Y. Li, V.P. Dravid, J. Am. Chem. Soc. 125 (2003) 9930.
[9] S.H. Hong, C.A. Mirkin, Science 288 (5472) (2000) 1808.
[10] L.M. Demers, D.S. Ginger, S.-J. Park, Z. Li, S.-W. Chung, C.A. Mirkin, Science 298 (2002) 1836.
[11] L.M. Demers, S.J. Park, T.A. Taton, Z. Li, C.A. Mirkin, Angew. Chem. Int. Ed. 40 (16) (2001) 3071.
[12] H. Zhang, S.W. Chung, C.A. Mirkin, Nano Lett. 3 (1) (2003) 43.
[13] S.H. Hong, J. Zhu, C.A. Mirkin, Langmuir 15 (23) (1999) 7897.
[14] S.H. Hong, J. Zhu, C.A. Mirkin, Science 286 (5439) (1999) 523.
[15] A.D. Barone, J.E. Beecher, P.A. Bury, C. Chen, T. Doede, J.A. Fidanza, G.H. Mcgall, Nucleosides Nucleotides Nucleic Acids 20 (2001) 525.
[16] K.B. Lee, J.H. Lim, C.A. Mirkin, J. Am. Chem. Soc. 125 (19) (2003) 5588.
[17] K.-B. Lee, S.J. Park, C.A. Mirkin, Science 295 (2002) 1702.
[18] H. Zhang, Z. Li, C.A. Mirkin, Adv. Mater. 14 (20) (2002) 1472.
[19] H. Zhang, C.A. Mirkin, Chem. Mater. 16 (2004) 1480.
[20] D.A. Weinberger, S.G. Hong, C.A. Mirkin, B.W. Wessels, T.B. Higgins, Adv. Mater. 12 (21) (2000) 1600.
[21] X. Liu, L. Fu, S. Hong, V.P. Dravid, C.A. Mirkin, Adv. Mater. 14 (2002) 231.
[22] L.M. Demers, C.A. Mirkin, Angew. Chem. Int. Ed. 40 (16) (2001) 3069.
[23] D.S. Ginger, H. Zhang, C.A. Mirkin, Angew. Chem. Int. Ed. 43 (2004) 30.
[24] S. Rozhok, R. Piner, C.A. Mirkin, J. Phys. Chem. B 107 (3) (2003) 751.
[25] P.E. Sheehan, L.J. Whitman, Phys. Rev. Lett. 88 (2002) 156104.
[26] B.L. Weeks, A. Noy, A.E. Miller, J.J. De Yoreo, Phys. Rev. Lett. 88 (2002) 255505.
[27] J. Jang, S. Hong, G.C. Schatz, M.A. Ratner, J. Chem. Phys. 115 (6) (2001) 2721.
[28] A.W. Adamson, Physical Chemistry of Surfaces, Wiley Interscience, New York, 1990.
[29] S. Morita, S. Fujisawa, Y. Sugawara, Surf. Sci. Rep. 23 (1996) 3.
[30] R.W. Carpick, M. Salmeron, Chem. Rev. 97 (1997) 1163.
[31] H. Zhang, R. Elghanian, N.A. Amro, S. Disawal, R. Eby, Nano Lett. 4 (2004) 1649.
[32] R.D. Piner, C.A. Mirkin, Langmuir 13 (1997) 6864.
[33] Y. Zhang, K. Salaita, J.H. Lim, C.A. Mirkin, Nano Lett. 2 (12) (2002) 1389.